www.vbripress.com, www.amlett.com, DOI: 10.5185/amlett.2012.2321 Published online by the VBRI press in 2012

Synthesis and chracterization of a tungsten bronze ferroeletcric oxide

B. N. Parida, Piyush R. Das*, R. Padhee and R. N. P. Choudhary

Department of Physics, Institute of Technical Education and Research, Siksha O. Anusandhan University, Bhubaneswar 751030, India

*Corresponding author. Tel: (+91) 9438047597; Fax: (+91) 6742351217; E-mail: prdas63@gmail.com

Received: 13 February 2012, Revised: 03 April 2012 and Accepted: 16 April 2012

ABSTRACT

A new ferroelectric oxide ($Li_2Pb_2Gd_2W_2Ti_4Nb_4O_{30}$) of the tungsten bronze structural family was synthesized using a high temperature solid-state reaction (i.e., mixed-oxide) method at 1100°C. Room temperature structural analysis (XRD) shows the formation of a new compound in single phase. The ferroelectric phase transition temperature (much above the room temperature) was determined by the dielectric and polarization measurements. Impedance, modulus and electrical conductivity of the material exhibit a strong correlation between its micro-structure and electrical parameters. The existence of non-exponential-type of conductivity relaxation in the compound was confirmed by detailed studies of its transport properties.

Keywords: Ceramics; x-ray method; microstructure; ferroelectricity/ferroelectric material; impedance.

B. N. Parida is a postgraduate (1996) in Physics from Sambalpur University. He is pursuing his PhD in Physics (Condense Matter). He is presently working as Lecturer in the Department of Physics, Institute of Technical Education & Research (Siksha 'O' Anusandhan University), Bhubaneswar, Odisha. His major field of research is in the area of ferroelectric materials.

P. R. Das is a postgraduate (1987) in Physics from Ravenshaw college, Cuttack. He did his PhD in Physics (Condense Matter) from IIT Kharagpur in 2008. He is presently working as Associate Professor in the Department of Physics, Institute of Technical Education & Research (Siksha O Anusandhan University), Bhubaneswar, Orissa. His major field of research is in the area of multiferroics/ferroelectric materials. He is presently guiding several research students for PhD degree.

R. Padhee is a postgraduate (2003) in Physics from National Institute of Technology, Rourkela. He is pursuing his PhD in Physics (Condense Matter). He is presently working as Sr.Lecturer in the Department of Physics, Institute of Technical Education & Research (Siksha 'O' Anusandhan University), Bhubaneswar, Odisha. His major field of research is in the area of ferroelectric materials and semiconductors.

Introduction

The discovery of interesting non-linear dielectric property (i.e., ferroelectricity) in $BaTiO_3$ attracted attention of scientists to examine ferroelectric properties of a large number of compounds of similar and/or different structural family useful for device applications [**1, 2**]. Among all the ferroelectric oxides known today, some ferroelectrics of perovskite and tungsten bronze (TB) structural families are found to be important for piezoelectric, pyroelectric and ferroelectric devices above room temperature. Because of the structural simplicity and stability of ABO_3-type (A = mono-divalent ions, B = tri-hexavalent ions) perovskite ferroelectrics some of them have widely been used for their basic understanding and applications. Though another class of ferroelectric oxides of the tungsten bronze (TB) structure of a general formula $[(A_1)_2(A_2)_4](C)_4[(B_1)_2(B_2)_8]O_{30}$ (where A-sites are occupied by mono to tri-valent cations, B-sites are occupied by tetra-hexavalent ions and C-sites is often empty), are complex and disordered, they have also been found much more useful for many devices. The properties of this type of materials can be tailored by making suitable modifications/ substitutions at A, B or/and C sites. In view of the above, some TB structured ferroelectrics have been found special in the family of oxide-materials for device applications. Because of the importance of the TB structured materials, a large number of compounds of this family have been studied in the past in the form of single crystal, thin film or/and ceramic form. Structural, ferroelectric and electrical transport properties of some compounds (related to this paper) such as $Pb_3R_3Ti_5Nb_5O_{30}$ (R = rare earth ion) have been studied by several workers [**3-7**]. Attempts have also been made to develop some

ferroelectrics with multi-valence complex TB structure [**8-11**] to enhance some of their properties. It is now known that many complex or disordered compounds provide interesting properties. Detailed literature survey shows that not much work have been done on the compounds having all six valence ions. Recently, structural and electrical properties of Ca modified $Ba_5NdTi_3Nb_7O_{30}$ [**12**] and dielectric and pyro-electric properties of $Ba_5SmTi_3Nb_7O_{30}$ [**13**] have been reported. More recently ferroelectric and related properties of $Li_2Pb_2Pr_2W_2Ti_4Nb_4O_{30}$ (LPPWTN) have been reported by Parida et al [**14**]. The dielectric constant, tangent loss and disordering in the compound were found to be higher than those of other TB compounds, whereas the value of $2P_r$ and $2E_c$ decreases with rise in temperature. As the ferroelectric and related properties in the $Li_2Pb_2Gd_2W_2Ti_4Nb_4O_{30}$ (LPGWTN) complex system is not known, we have synthesized and studied various properties of the material.

Experimental

The polycrystalline sample of $Li_2Pb_2Gd_2W_2Ti_4Nb_4O_{30}$ (LPGWTN) was synthesized using a high- temperature solid-state reaction technique with high-purity (AR grade) ingredients: Li_2CO_3, TiO_2, Nb_2O_5 and WO_3 (99%, all from M/s LOBA Chemie Pvt. Ltd. India), PbO (99.9% M/s E Merk India Ltd), Gd_2O_3 (99.9%, M/s Indian rare earth Ltd). These oxides and carbonate were mechanically mixed in dry (air) and wet (methanol) medium for several hours in agate mortar. The mixed material was calcined at an optimized temperature (1100 °C) for 4 h in alumina crucible. An X-ray diffraction (XRD) pattern of calcined powder was recorded at room temperature using X-ray powder diffractometer (Rigaku, Miniflex). The CuK_α radiation (λ=1.5405Å) was used to collect data in a wide range of Bragg's angles (θ) ($20^0 \leq 2\theta \leq 80°$) at a scanning rate of 3 deg/min for preliminary structural analysis. Using PVA (binder)-mixed (calcined) powder the cylindrical pellets (diameter 10 mm and 1-2 mm thickness) were fabricated under a uni-axial pressure of $4x10^6$ Nm^{-2} (with a hydraulic press). All the pellets were then sintered at an optimized temperature (1150 °C) in air atmosphere for 4 h to get mechanically stable, strong and high density (> 95% of theoretical density) samples. The polished-sintered pellets were electrode with high purity and quality silver paste and, dried at 160 °C for 8 h before taking dielectric and electrical measurements. The surface morphology of a gold-coated pellet sample was recorded by JEOL JSM-5800 scanning electron microscope (SEM). The capacitance, dissipative factor, and impedance parameters of silvered-coated pellet were measured as a function of temperature (25-500 °C) in a wide range of frequency (1 kHz-1MHz) using a computer-controlled impedance meter (PSM-4NL Model: 1735, UK) with a laboratory-designed and fabricated sample holder and furnace. To record the temperature at small interval, a chromel-alumel thermo-couple and KUSAM MECO 108 digital milli-voltmeter were used. The hysteresis loop of the compound on its poled (electric field= 12 kV/cm, time = 8 h) sample were recorded at different temperatures using a loop tracer (M/S Marine India, New Delhi). Because of the experimental limitation on temperature, hysteresis loop above 200°C could not be obtained to determine the ferroelectric-paraelectric phase transition. However, decreasing trend in the value of remnant polarization and area of the hysteresis loop on increasing temperature (towards transition temperature) is an indication of the existence of ferroelectric property in the material.

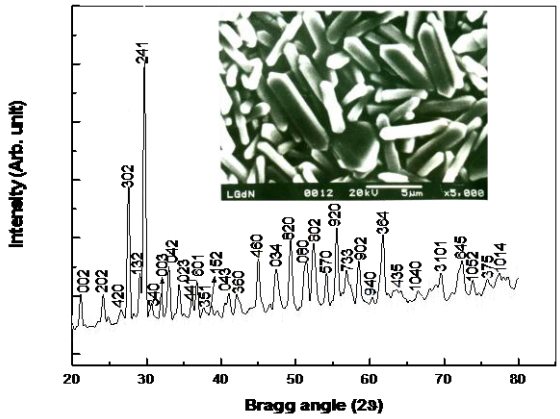

Fig. 1. Indexed XRD pattern and SEM micrograph of LPGWTN.

Results and discussion

Structural analysis

The X-ray diffraction (XRD) pattern of $Li_2Pb_2Gd_2W_2Ti_4Nb_4O_{30,}$ recorded at room temperature on its powder sample, is shown in **Fig. 1.** The XRD pattern consists of many sharp and single peaks, which are different from those of the ingredients. The XRD pattern clearly exhibits better homogeneity and crystallization of the sample, and thus confirms the formation of new compound [**15**] in a single phase. Since TB structure is generally crystallized in tetragonal or orthorhombic structure, most of the peaks of XRD pattern were indexed in these two systems with different unit cell configurations using a standard computer program package "POWD" [**16**]. A good agreement between observed (obs.) and calculated (cal.) inter planar spacing of each reflection were found to be in a particular unit cell configuration of orthorhombic crystal system. The selected lattice parameters (a, b and c) of a unit cell were refined using a least-squares refinement sub-routine of POWD. The refined lattice parameters of the material are found to be consistent with those of some reported compounds of TB structure family [**11**]. Further, the crystallite or particle size (P) of the compound was calculated using the broadening of some widely spread (over Bragg angles) strong and medium reflections in the Scherrer's equation [**17**]:

$$P_{hkl} = \frac{K\lambda}{\beta_{1/2} Cos\theta_{hkl}}$$

where k (constant) = 0.89, λ=1.5405Å and $\beta_{1/2}$= full width at half maximum (in radians). The average value of P_{hkl} is found to be 13 nm. The least-squares refined unit cell parameters are: a = 15.2957(13) Å, b= 14.1981(13) Å, c = 8.3946(13) Å and volume V = 1823.05 $Å^3$ (the numbers

indicated in parenthesis are estimated standard deviation in unit cell parameters). The orthorhombic distortion, calculated by: δ= [b-a/b+a] equation was found to be 0.0372. As the TB structure is built on five crystallographic sites, it is difficult to precisely determine the Gd^{+3} ions coordination (12- or 15- fold coordination) based on the current results. However, the numerous structural studies show that the rare -earth ions predominately prefer the A_1 tunnels [**8**].

The SEM micrograph of LPGWTN is shown in **Fig. 1** (inset).The nature (size, shape and distribution of grains) of the microstructures of the sample suggests that the grain growth has more or less completed during sintering, and hence no secondary phase was observed. Because of some voids of irregular shape, size and dimension very high density sample could not be obtained. In addition to the above, some small size grains were found to be homogenously distributed throughout the surface of the sample. The grain size (from the micrograph) is found to be in the range of 2-8 μm.

Dielectric study

The variation of relative dielectric constant (ε_r) and tangent loss (tanδ) as a function of temperature at some selected frequency (10kHz, 100kHz and 1MHz) is shown in **Fig. 2a** (inset).The value of ε_r increases on increasing temperature up to a temperature (usually referred as transition temperature (T_c)), and then decreases. The variation of tanδ with temperature follows the similar trend as of ε_r. This compound has two phase transitions: T_{c1} and T_{c2}. The lower transition temperature (T_{c1}= 325°C) may be considered as ferroelastic to ferroelectric, whereas the upper one (T_{c2}= 402.5°C) may be due to the ferroelectric to paraelectric phase transition [**18**]. It is observed that the values of ε_{max} (dielectric constant at T_{c1}) at 10, 100, and 1000 kHz are found to be 446, 345, 277, and those of at T_{c2} are 501, 340, 287 respectively which are much higher than that of reported similar compound, $Na_2Pb_2Nd_2W_2Ti_4Nb_4O_{30}$ [**10**].

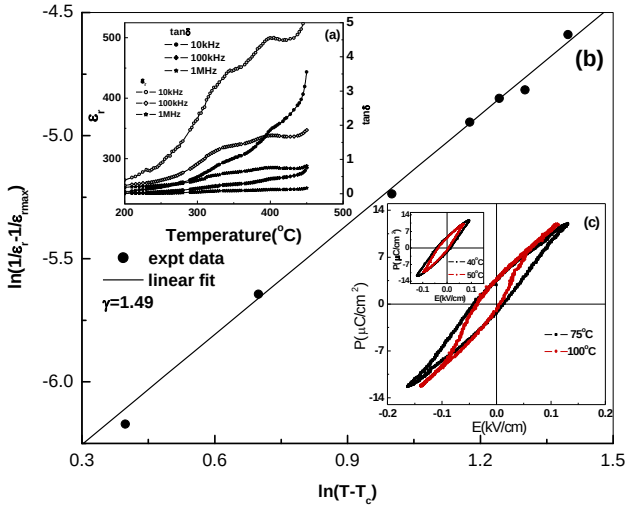

Fig. 2. Variation of (a) ε_r and tanδ with temperature and frequency,(b) ln $(1/\varepsilon_r - 1/\varepsilon_{max2})$with ln (T-Tc2) and (c) polarization with electric field at different temperature of LPGWTN.

The values of $\tan\delta_{max1}$ (tangent loss at Tc1) at same frequency are found to be 1.01, 0.28, 0.1 and those of at T_{c2} are 1.91, 0.46, 0.15 respectively. The rate of increase of tanδ with temperature in the material is smaller in the low temperature region, but at higher temperatures this rate increases sharply. The sharp increase in the value of tanδ at higher temperatures may be due to scattering of thermally activated charge carriers, and some inherent or developed defects in the sample during processing at high temperatures. At higher temperatures the conductivity begins to dominate, which in turn, is responsible for rise in tanδ. The values of ε_{max2} and $\tan\delta_{max2}$ of the titled compound decrease with rise in frequency. Such a characteristic is normally found in ferroelectric oxide materials. This is because of the absence of dipolar and ionic polarizations in the material at higher frequency. Additionally, dispersion in tanδ at higher temperatures was observed (**Fig. 2a**). This trend has also been observed in similar-type of compounds [**9-11**]. This change may be associated to ionic conductivity of the material which is related to loss of oxygen or PbO at higher temperatures during processing. Some dielectric peaks were found to be broadened or diffused. In order to estimate the degree of diffuseness/disorder in the dielectric peaks of the compound, a general expression [**19**]:

$$\frac{1}{\varepsilon_r} - \frac{1}{\varepsilon_{max2}} \alpha (T - T_{c2})^{\gamma}$$

$$\ln\left(\frac{1}{\varepsilon_r} - \frac{1}{\varepsilon_{max2}}\right) = \gamma \ln(T - T_{c2}) + constant$$

It is normally used, where ϵ_r is relative dielectric constant at a temperature T and ϵ_{max2} is its maximum value at T_{c2}. The value of diffusivity (γ) was calculated from the slope of the curve (**Fig. 2b**). When the value of diffusivity varies between 1 (obeying Curie-Weiss law) and 2 (for completely disordered system), the existence of diffuse phase transition in the material is confirmed. As the calculated value of diffusivity is found to be γ =1.49 in the material, the presence of diffuse phase transition in the material is confirmed. The diffuse phase transition is usually observed in TB structured ferroelectrics, which can be explained by the presence of certain non-equivalent position in the unit cell [**20**]. It is known that the TB structured compounds loose oxygen during high-temperature sintering [**13**] which can be represented by using Kröger and Vink notation [**21**]

$$O_o \rightarrow 1/2\ O_2\uparrow + V_o'' + 2e^-$$

where V_o'' denotes oxygen vacancies. The defects such as oxygen vacancies V_o'' induce disorderness in the system [**22**] as a result diffuse type phase transition occurs.

Polarization study

The P-E hysteresis loops of LPGWTN at different temperatures are shown in **Fig. 2c** (inset). The remnant polarization ($2P_r$) of the compound at 40, 50, 75 and 100°C was found to be 6.38, 5.3, 5, 4.61 μC/cm^2 respectively. The value of E_c at these temperatures was found to be 0.056, 0.045, 0.043, 0.036 kV/cm respectively. It is clear that the compound has low coercive field and small remnant

polarization. The decreasing trend in remnant polarization and area of the loop with rise in temperature confirms the existence of ferroelectric properties in the material. The transition temperature could not be determined from hysteresis study because of our experimental limitations on temperature.

Impedance and modulus spectroscopy

Impedance spectroscopy (IS) is a non-destructive technique to characterize ferroelectric and ionic crystals/materials as a function of frequency and temperature. This technique is more useful to separate the contributions of (i) bulk, (ii) grain boundary and (iii) electrode polarization effects of the above types of materials. An ac signal is applied across the electroded-pellet sample, and its output response is measured. Measurements of impedance and related parameters of the materials provide us some important data having both real (resistive) and imaginary (reactive) components. These components are calculated using some basic equations: complex impedance

$$Z(\omega) = Z' - jZ'' = R_s - \frac{j}{\omega C_s}$$

and the complex electrical modulus

$$M(\omega) = \frac{1}{\varepsilon(\omega)} = M' + j\,M'' = j\,\omega C_0 Z$$

complex admittance

$$Y^* = Y' + jY'' = j\omega C_0 \varepsilon^* = (R_p)^{-1} + j\omega C_p$$

And complex permittivity $\varepsilon^* = \varepsilon' - j\varepsilon''$ where $\omega = 2\pi f$ is the angular frequency; C_0 is the geometrical capacitance, $j = \sqrt{-1}$ and subscripts p and s are parallel and series circuit components respectively. The peak of the high frequency semicircular arc in the complex impedance spectra enables us to calculate the relaxation frequency (ω_{max}) of the bulk material using the equation:

$$\omega_{max}\tau = \omega_{max} R_b C_b = 1 \Rightarrow 2\pi f_{max} R_b C_b$$

where R_b= bulk resistance and C_b= bulk capacitance.

Impedance analysis

Fig. 3a shows the variation of Z' with Z" (usually referred as Nyquist plot) at selected temperatures of LPGWTN over a wide range of frequency (1 kHz–1MHz). The impedance is characterized by the appearance of temperature dependence of semicircular arcs. At lower temperatures, complex impedance plots show the trend or/and formation of single semicircular arc (not shown here). At higher temperatures (>350 ^{o}C) two semicircular arcs (with centre below the real axis) are observed. Most appropriate approach to interpret the depression of semicircles is statistical distribution of relaxation time [**23**].

The nature of plots suggests that the electrical response is composed of at least two semicircles; first due to bulk (grain) property of the material whereas the second one (at high temperature) is due to contributions of grain boundary [**24**]. **Fig. 3(a)** (inset) shows comparison of experimental and fitted impedance data using commercially available software (ZSIMP WIN version 2.0). In Debye-like response, an equivalent circuit consists of series combination of (CQR) and (CR) where Q is known as a constant phase element (CPE). The admittance of CPE is defined as

$$Y\,(CPE) = A_0\,(j\omega)^{\,n} = A\omega^n + jB\omega^n$$

with $A = A_o \cos(n\pi/2)$ and $B = A_o \sin(n\pi/2)$ where A_0 and n are frequency independent but temperature dependent parameters. A_0 is the magnitude of the dispersion, and $0 \le n \le 1$ (for an ideal capacitor n=1, and for ideal resistor n = 0) [**25**].

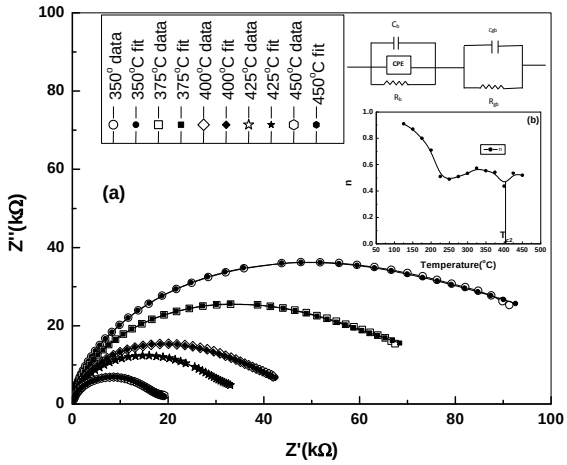

Fig. 3. Variation of (a) Z' with Z" and (b) n with temperature of LPGWTN

The temperature variation of n is shown in **Fig. 3b** (inset). The value of n decreases and becomes minimum near T_{c2}. Because of the absence of one of the transverse (soft) modes, restoring force tends to zero at the ferroelectric-paraelectric phase transition [**26**]. If charge carrier is coupled with soft mode, it becomes mobile near phase transition. From this fitted curves, the values of R_b (bulk resistance), R_{gb} (grain boundary resistance), bulk capacitance (C_b) and grain boundary capacitance (C_{gb}) at different temperatures were calculated and compared (**Table 1**). It clearly shows that the parameters R_b, R_{gb} and C_b decrease with rise in temperature implying the existence of negative temperature co-efficient of resistance (NTCR) in the material [**27**]. The value of C_{gb} increases with rise in temperature because of its interfacial effect [**28**].

Table 1. Comparison of bulk (grain) and grain boundary resistance and capacitance at different temperatures.

Temp. (^{o}C)	R_b (Ω)	C_b (nF)	R_{gb} (Ω)	C_{gb} (nF)
325	151500	0.1343	27520	0.7244
350	102400	0.1255	15470	12.23
375	73470	0.1163	9907	18.45
400	43020	0.1066	4970	44.22
425	34100	0.1063	3850	45.3
450	18850	0.1061	1969	62.29

A semi-circle with its center at Z' axis is observed for an ideal Debye-type relaxation. In the studied material Debye-type of relaxation is not observed. The depressed semi-circles indicate the presence of non–Debye type of relaxation. There is a distribution of relaxation time instead of a single relaxation time in the material [**29, 30**]. The intercept of each semi-circle on real Z' axis measures the contributions of bulk and grain boundary effect. The semi-circles of the impedance spectrum have a characteristic peak occurring at a unique relaxation frequency (i.e., relaxation frequency (f_r) ($\omega_r = 2\pi f_r$)). It can be expressed as ω_r RC = $\omega_r\tau$ = 1, where τ is the relaxation time. The value of relaxation time due to bulk (τ_b) and grain boundary (τ_{gb}) was calculated using the equation $\omega_r\tau = 1$ or, $\tau = 1 / 2\pi f_r$ = RC. The variation of $\ln\tau_b$ and $\ln\tau_{gb}$ with inverse of temperature (10^3/T) is shown in **Fig. 4a**. It is observed that the value of τ_b and τ_{gb} decreases with rise in temperature, and thus temperature dependence of relaxation time follows the Arrhenius relation: $\tau = \tau_o \exp(-E_a/k_BT)$ where τ_o is the pre-exponential factor, k_B is Boltzmann constant and T is the absolute temperature. The calculated values of activation energy (E_a) are 1.12eV and 1.18eV respectively. In **Fig. 4** (b, c) (inset), the values of R_b, R_{gb}, C_b and C_{gb} are plotted against inverse of temperature which gives the Arrehenius plots. In **Fig. 4b** the increasing nature of σ_{dc} with rise in temperature supports the NTCR (negative temperature coefficient of resistance) behavior of the sample. The nature of the plot follows the Arrhenius relation [**25**]

$$\sigma_{dc} = \sigma_o \, e^{-\frac{E_g}{kT}}$$

The slope of these plots gives bulk and grain boundary conduction activation energy respectively. The values of activation energy have been compared in **Table 2**. It is seen that conduction mechanism is basically dominated by grain boundary conduction through hopping electrons created due to oxygen vacancy [**31**].

Fig. 5a (inset) shows the variation of Z' and Z" as a function of frequency at some selected temperatures. The value of Z' decreases with rise in frequency and temperature which is related to the electrical conductivity of the material.

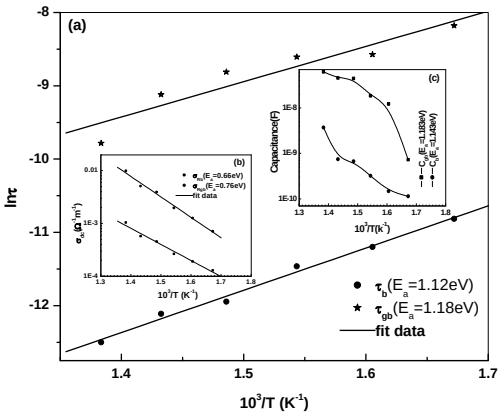

Fig. 4. (a-c) Variation of lnτ, Sigma DC and Capacitance with inverse of the absolute temperature (103/ T) of LPGWTN.

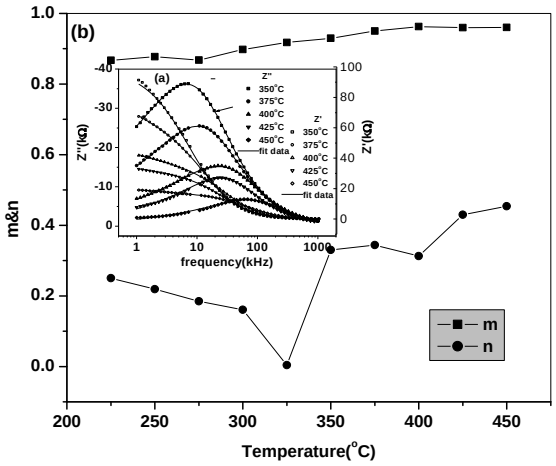

Fig. 5. (a-b). Variation of Z' and Z" with frequency of LPGWTN.

Table 2. Comparison of bulk (grain) and grain boundary conductions and relaxation activation energies.

T (325-450°C)	Bulk conduction (E_a)(eV)	Grain boundary conduction (E_a)(eV)
Relaxation (τ)	1.12	1.18
Resistance (σ_{dc})	0.66	0.76
Capacitance (C)	1.143	1.183

At high frequency the value of Z' of each temperature coincides implying the possible release of space charge [**32**]. At high temperatures, it is observed that with increase in frequency the value of Z" increases to a maximum ($Z"_{max}$) and then decreases. This explains the presence of relaxation in the sample [**33**]. The broadening of $Z"_{max}$ peak with increase of temperature is a clear indication of the occurrence of temperature dependence of relaxation phenomenon in the material. The relaxation process occurs due to the presence of immobile charges at low temperatures and inherent defects and vacancies created during higher temperature processing of the sample [**28, 34**].

The imaginary part of the impedance plot indicating high frequency slopes is independent of temperature. On the other hand, low frequency slopes are strongly temperature dependent. These two temperature dependence of slopes suggest that there are two distinct dispersion mechanism involved in the sample. The asymmetric behavior, which is similar to other ferroelectrics [**26, 35**], can be explained using the equivalent circuits: CQR for low temperature and (CQR) (CR) for high temperature) as shown in **Fig. 3** (inset) where $C = A(j\omega)^{m-1}$ and $Q = A(j\omega)^{n-1}$ are Jonscher's universal capacitances [**36**]. The frequency dependence of the AC complex impedance can be expressed as;

$$Z^* = \frac{R_o}{1+\left(\frac{j\omega}{\omega_1}\right)^m + \left(\frac{j\omega}{\omega_2}\right)^n} \quad [26]$$

where $\omega_1 = 2\pi f_1$ and $\omega_2 = 2\pi f_2$ are the first and second characteristic angular frequencies respectively, exponent m for high frequency and n for low frequency. An excellent agreement between experimental and calculated values of both real and imaginary parts of impedance is observed

from non-linear curve fitting as shown in **Fig. 5a** (using the formula [**26**]).

$$Z'' = \frac{K_o}{\left(\frac{\omega}{\omega_1}\right)^m + \left(\frac{\omega}{\omega_2}\right)^{-n}}$$

The variation of fitting parameters (m and n) with temperature is shown in **Fig. 5b**. This plot (m vs. temperature) confirms that it is close to unity and temperature independent. On the other hand the value of n is less than one, and is temperature dependent. In the ferroelastic state the value of n decreases and it attains minimum at $T_{c1,}$ and subsequently increases at few temperatures and suddenly goes to a minimum at T_{c2}. The minimum and maximum value of n at two different temperatures (T_{c1} andT_{c2}) once again can be explained by restoring force between charge carriers and lattice [**26**]. The above variation in the value of n can also be understood by the theory given by Dissado and Hill [**37, 38**]. According to them, the exponent n characterizes the magnitude of the correlation in a single dipole reorientation. The unity value corresponds to fully correlated transitions and zero value corresponds to fully uncorrelated transition. In our experiment n tends to minimum at T_{c1} and T_{c2} suggesting a strongly uncorrelated reorientation of the charge carrier polarization at transition points.

Modulus analysis

The electrode/polarization and grain boundary conduction effect in the materials can easily be distinguished using electrical modulus analysis. It can also detect bulk properties as apparent conductivity and relaxation time [**24, 39**]. **Fig. 6a-b** shows the variation of M' and M" with frequency at some selected temperatures.

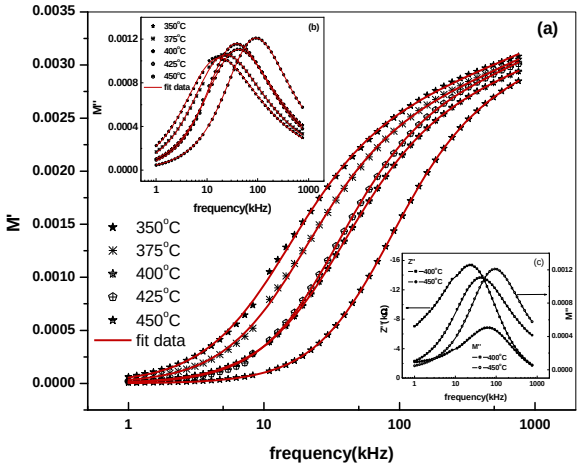

Fig. 6. Variation of (a) M', (b) M" and (c) Z" & M" with frequency at different temperatures of LPGWTN.

The value of M' approaches to zero in the low frequency range confirming the presence of an appreciable electrode and/or ionic polarization in the studied temperature. An observation of monotonic dispersion with rise in frequency may be due to the presence of short range mobility of charge carriers. This implies that there is a lack of restoring force for flow of charges under the influence of steady electric field [**40**].The variation of M" with frequency at different temperatures in **Fig. 6b** (inset) reveals that as frequency increases M" increases and takes peak value at a particular frequency beyond 250°C (not shown in fig.).This trend will continue, however the value of M" decreases with increase in temperature. The peak value of M" for 325°C is much less than compared with the same at other temperatures indicating that 325°C is the ferroelastic to ferroelectric transition temperature of the sample. Beyond 350°C, the trend of M" peak increases and attain minimum at 400°C which is the ferroelectric to paraelectric phase transition temperature [**31**]. The peak position of M''_{max} shifts towards higher frequency side indicates the temperature dependent of dielectric relaxation, which clearly suggests that in thermally activated process, the hopping mechanism of charge carriers dominates. Asymmetric broadening of the peak shows the spread of relaxation with different time constants, and hence the relaxation in the material is considered to be of non-Debye- type [**25**]. The frequency dependence of the AC complex impedance can be expressed as [**26**];

$$Z^* = \frac{R_o}{1+\left(\frac{j\omega}{\omega_1}\right)^m + \left(\frac{j\omega}{\omega_2}\right)^n}$$

where $\omega_1 = 2\pi f_1$ and $\omega_2 = 2\pi f_2$ are the first and second characteristic angular frequencies respectively. A similar type of relation is used for complex modulus which can be expressed as [**41**];

$$M^* = \frac{C_0^{-1}}{1+\left(\frac{j\omega}{\omega_1}\right)^m + \left(\frac{j\omega}{\omega_2}\right)^n}$$

An excellent agreement between experimental and calculated values for both real and imaginary parts of modulus is observed from non-linear curve fitting as shown in **Fig. 9a-b** (using the formula [**26, 41**]).

$$M'' = \frac{C_0^{-1}}{1+\left(\frac{j\omega}{\omega_1}\right)^m + \left(\frac{j\omega}{\omega_2}\right)^{-n}}$$ [**26, 41**].

The impedance (Z") and modulus (M") spectroscopy plot are shown in fig.6(c) (inset). The combine plots of Z" and M" as a function of frequency are used to detect presence of smallest capacitance and largest resistance as suggested by Sinclair et.al [**42**]. This will help whether relaxation process is short range or long range motion of charge carriers. If the process is short range, peaks of Z" and M"~ frequency are occur at different frequencies otherwise for long range movement of charge carrier peaks are occur at same frequencies[**23, 43**]. In the studied compound there is mismatch of peaks at different temperature suggests short range motion of charge carrier and departure from ideal Debye-like behavior [**23**].

AC conductivity

Detailed studies of ac conductivity are carried out for the better understanding of the frequency dependence of electrical properties of the material. Measurements of frequency dependence of ac conductivity also provide information regarding the nature of charge carriers. The ac electrical conductivity (σ_{ac}) was calculated using the dielectric data and an empirical relation, $\sigma_{ac} = \omega \varepsilon_r \varepsilon_0 \tan\delta$, where ε_0 is permittivity in free space and ω is angular frequency. In order to have better understanding of conduction mechanism in the material, we have to follow Jonscher's universal power law [**34**]:

$$\sigma_T(\omega) = \sigma(0) + \sigma_1(\omega) = \sigma_0 + A\omega^n$$

where $\sigma(0)$ is the frequency independent term giving dc conductivity and $\sigma_1(\omega)$ is the purely dispersive component of ac conductivity. The value of exponent (n) of the above equation can be between zero and one depending on temperature and materials but independent of frequency.

Fig. 7 shows the variation of σ_{ac} with frequency at a few selected temperatures. It is observed that σ_{ac} increases with rise in frequency at higher temperature. At low temperatures, it is nearly frequency independent. The extrapolation of this part towards lower frequency side gives σ_{dc}. The increasing trend of σ_{ac} with rise in frequency (in low frequency region) may be attributed to the disordering of cations between neighboring sites, and presence of space charge. In the high frequency region the curves approach each other. The nature of conductivity plots reveals that the curves exhibit low frequency dispersion phenomena obeying the Jonscher's power law [**34**].

The origin of the frequency dependence of conductivity lies in the relaxation phenomena arising due to mobile charge carriers [**34**]. When a mobile charge carrier hops to a new site from its original position, it remains in a state of displacement between two potential energy minima.

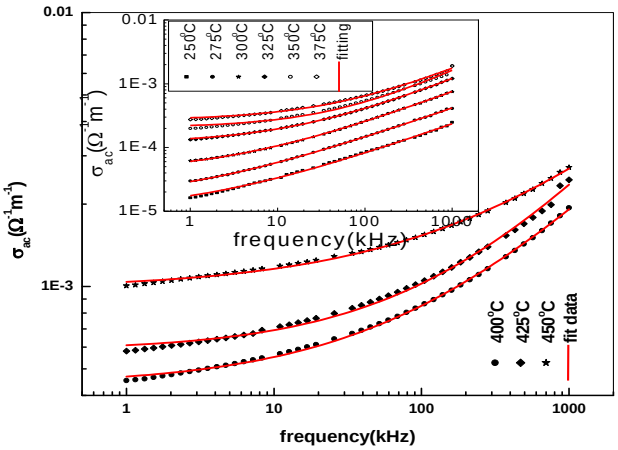

Fig. 7. Variation of ac conductivity with frequency at different temperatures.

The conduction behavior of the material obeys the power law; $\sigma(\omega) \alpha \omega^n$ with a slope change governed by 'n' in the low temperature region. The value of n less than 1 signifies that the hopping motion involves a translational motion with a sudden hopping whereas n > 1 represents the motion involves localized hopping without the species leaving the neighborhood. The frequency at which change in slope takes place is known as hopping frequency of the polarons (ω_p), and is temperature dependent. The low frequency dispersion has been attributed to the ac conductivity whereas the frequency independent plateau region corresponds to the dc conductivity. From non-linear fitting it is found that that motion of charge carriers is translational because of small value of n (< 1) [**44**]. In **Fig. 8a-b** the fitting parameters dc conductivity, 'A' and n are compared. **Fig. 8b** shows the variation of dc conductivity as a function inverse of absolute temperature which shows similar trend as mentioned in **Fig 4.** The calculated activation energy is found to be 0.73eV in high temperature region, which is consistent with that of calculated from **Fig. 4.**

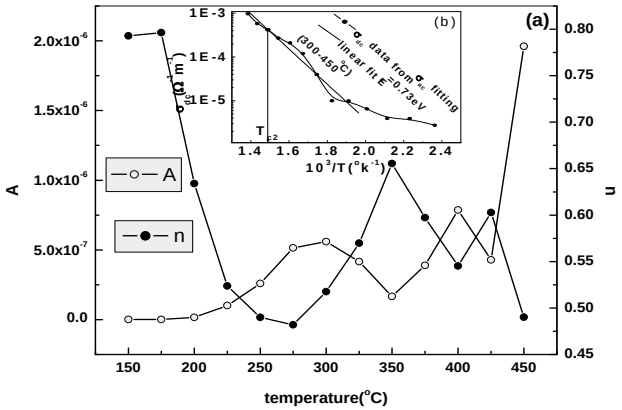

Fig. 8. Variation of (a) A and (b) dc conductivity as a function of temperatures.

Fig. 8a shows the variation of A and n as function of temperature. It is observed that value of n decreases with rise in temperature, and attains minimum at T_{c2}, and again it increases on further increase in temperature. In the titled compound the value of n becomes maximum at T_{c1} and minimum at T_{c2}. At the same time the values of pre-exponential factor A have reverse trend and attain minimum at T_{c1} and maximum at T_{c2}.The value of n represents degree of interaction between mobile ion and the lattices surround them [**45**]. With rise in temperature there is increase in interaction among the charge carriers and lattices which leads to decrease in n. The minimum value of n nearby at T_{c1} implies an interaction among charge carriers and lattices is less (ferroelastic to ferroelectric phase transition). On the other hand minimum value of n at T_{c2} shows minimum correlation between charge carriers and lattices (ferroelectric to paraelectric phase transition). The pre-exponential factor A determines the strength of polarizability. The minimum value of A at T_{c1} will have lower polarizability and the maximum value of A at T_{c2} implies higher polarizability (i.e., maximum dielectric constant).

Conclusion

The preliminary X-ray structural analysis of a solid-state reaction/mixed-oxide method- prepared sample of LPGWTN showed orthorhombic crystal structure of tungsten bronze-type at room temperature. Detailed studies of dielectric properties of the compound exhibit diffuse-type of multiple phase transitions. Complex impedance analysis of the compound shows that the material has (i) conduction due to bulk material up to temperature 400^{o}C, (ii) NTCR-type behavior and (iii) temperature dependent relaxation phenomena. The impedance spectrum has also been used to estimate the electrical conductivity. The activation energy of the sample, estimated from the conductivity pattern, relaxation time and modulus pattern, is almost the same. This indicates that the same type of charge carriers is available for both the electrical conduction and electrical relaxation phenomena in the sample. The activation energy due to grain boundary effect suggests the possibility of electrical conduction due to the mobility of the oxygen ions or vacancies. Modulus analysis indicates non–exponential type of conductivity relaxation in the material. The appearance of polarization–electric field hysteresis loop below transition temperature confirms the existence of ferroelectric properties of the material.

Reference

1. Barik, S K.; Singh, A.K.; Choudhary**,** R N P. Adv. Mat. Lett. **2011**, 2(6), 419. **DOI:** 10.5185/amlett.2011.2228
2. Sahoo, S.; Choudhary, R N P. Adv. Mat. Lett. **2012**, 3(2), 97. **DOI:** 10.5185/amlett.2011.4250
3. Singh, A K.; Choudhary, R N P. Ferroelectrics **2005**, 325, 7. **DOI:** 10.1080/00150190500326522
4. Kim, M S.; Lee, J H.; Kim, J J.; Lee, HY.; Cho, S H. J. Solid State Electrochem **2006**, 10, 18. **DOI:** 10.1007/s10008-005-0647-9
5. Fang, L.; Zhang, H.; Huang, TH.; Yuan, R.Z.; Liu, HX. J. Mat. Sci. **2005**, 40, 533. **DOI:** 10.1007/s10853-005-6122-2
6. Behera, B.; Nayak, P.; Choudhury, RNP. Mat. Lett. **2005**, 59, 3489. **DOI:** 10.1016/j.matlet.2005.06.019
7. Hornebecq, V.; Elissalde, C.; Reau, JM.; Ravez, J. Ferroelectrics, **2000**,238, 57. **DOI:** 10.1080/00150190008008767
8. Smolenskii, GA.; Agranovskaya, A I. Dokl. Akad. Nauk. SSSR, **1954**, 97, 237.
9. Das, Piyush R.; Pati, B.; Sutar, B.C.; Choudhury, R.N.P. Adv. Mat. Letts. **2012**, 3, 8. **DOI:** 10.5185/amlett.2011.4252
10. Das, PR.; Choudhary, RNP. ; Samantray, BK. J. Alloys. Comp. **2008**, 448, 32. **DOI:** 10.1016/j.jallcom.2006.10.090
11. Das, PR.; Choudhary, RNP. ; Samantray BK. J. Phys. Chem. Solids, **2007**, 68, 516. **DOI:** 10.1016/j.jpcs.2007.01.015
12. Ganguli, P.; Jha, A K. Int. Ferroelectrics **2010**, 115, 149. **DOI:** 10.1080/10584587.2010.488566
13. Ganguli, P.; Devi, S.; Jha, AK. Ferroelectrics **2009**, 381,111. **DOI:** 10.1080/00150190902870051
14. Parida, B N.; Das, Piyush R.; Padhee, R.; Choudhary, R N P. J. Phys. Chem. Solids **2012**, 73, 713 **DOI:**10.1016/j.jpcs.2012.01.013
15. Klug, H P.; Alexander, LE. Wiley Chester (England) **1974**, 966.
16. POWD E W, An interactive Powder diffraction data interpretation and indexing Program, Ver 2.1, School of Physical Science, Finders University of South Australia, Bedford Park, S.A. 5042, Australia.
17. Cullity, BD. Elements of X-ray Diffraction, Addison Wesley, **1978**.
18. Fang, L.; Zhang, H.; Wu, B.; Yuan, RZ. Progs. Crys. Growth Charac. Mat. **2000**, 40,161. **DOI:** 10.1016/S0960-8974(00)00037-1
19. Pilgrim, SM.; Sutherland, A E.; Winzer, SR. J. Am. Ceram. Soci. **1990**, 73, 3122. **DOI:** 10.1111/j.1151-2916.1990.tb06733.x
20. Cross, LE. Ferroelectrics **1987**, 76, 241. **DOI:** 10.1080/00150198708016945
21. Kröger, F.A.; Vink, H.J. Solid State Phys. **1956**, 3,307. **DOI:** 10.1016/S0081-1947(08)60135-6
22. Raghavan, V. Material Science and Engineering. New Delhi: Prentice-Hall of India, **2004**.
23. Nobre, M A L.; Lanfredi, S. J. Appl. Phy. **2003**, 93, 5557. **DOI:** 10.1063/1.1564281
24. Das, P S.; Chakraborty, PK.; Behera, B.; Choudhary, RNP. Phys. B. **2007**, 395, 98. **DOI:** 10.1016/j.physb.2007.02.065.
25. Macdonald, JR. Solid State Ionics **1984**, 13, 147. **DOI:** 10.1016/0167-2738(84)90049-3
26. Lu, Z.; Bonnet, J.P.; Ravez, J.; Reau, J.M.; Hagenmuller,P. J. Phys.Chem.Solids **1992,** 53, 1. **DOI:** 10.1016/0022-3697(92)90004-W
27. Ranjan, R.; Kumar, R.; Kumar, N.; Behera, B.; Choudhury, RNP. J. Alloys. Comp. 2011, 509, 6388. **DOI:** 10.1016/j.jallcom.2011.03.003
28. Suman, C K.; Prasad, K.; Choudhary, R.N.P. J. Mater. Sci. **2006**, 41, 369. **DOI:** 10.1007/s10853-005-2620-5
29. Sen, S.; Choudhary, RNP.; Pramanik, P. Phys. B, **2007**, 387, 56. **DOI:** 10.1016/j.physb.2006.03.028
30. Behera, B.; Nayak, P.; Choudhary, RNP. J. Alloys Comp. **2007**,436, 226. **DOI:** 10.1016/j.jallcom.2006.07.028
31. Rao, Sambasiva K.; Prasad, Madhava D.; Krishana, Murali P.; Tilak,B.; Varadarajulu,K.Ch. Mat. Sci. & Eng. B, **2006**, 133, 141. **DOI:** 10.1016/j.mseb.2006.06.030
32. Plocharski, J.; Wieczoreck, W. Solid State Ionics, **1988**, 28,979. **DOI:** 10.1016/0167-2738(88)90315-3
33. Behera, B.; Nayak, P.; Choudhary R N P. Mat. Res. Bull. 2008, 43, 401. **DOI:** 10.1016/j.materresbull.2007.02.042
34. Jonscher, AK. Nature **1977**, 267,673. **DOI:** 10.1038/267673a0
35. Kim, J S.; Kim, JN. Jpn. J.Appl.Phys. **2000**, 39, 3502. **DOI:** 10.1143/JJAP.39.3502
36. Jonscher, AK. "Dielectric Relaxation in solids" Chelesa Dielectric Press, London, **1983**.
37. Dissado, LA.; Hill, RM. Nature **1979**, 279, 685. **DOI:** *10.1038/279685a0*
38. Dissado, LA.; Hill, RM. Phill. Mag. B, **1980**, 41, 625. **DOI:** 10.1080/13642818008245413
39. Hodge, I M.; Ingram, M.D.; West, A.R. J. Electroanal. Chem. Interfacial Electroch **1975**, 58, 429. **DOI:** 10.1016/S0022-0728(75)80102-1
40. Macedo, P B.; Moynihan, CT.; Bose, R. Phys. Chem. Glasses, **1972**, 13,171.
41. Almond, D.P.; West, A.R., Solid state Ionics **1983**, 11, 57. **DOI:** 10.1016/0167-2738(83)90063-2
42. Sinclair, D C.; West, AR. J. Appl. Phys. **1989**, 66, 3850. **DOI:** 10.1063/1.344049
43. Pradhan, D K.; Choudhary, R N P.; Ranldi, C.; Katiyar, R S. J. Appl. Phys. **2009**,106, 024102. **DOI:** 10.1063/1.3158121
44. Funke, K. Prog. Solid State Chem. **1993**, 22, 111. **DOI:** 10.1016/0079-6786(93)90002-9
45. Lu, Z.; Bonnet, J P.; Ravez, J.; Hagenmuller, P. Solid State Ionics **1992**, 57, 235. **DOI:** 10.1016/0167-2738(92)90153-G

